

SEDformer: Event-Synchronous Spiking Transformers for Irregular Telemetry Time Series Forecasting

Ziyu Zhou¹, Yuchen Fang², Weilin Ruan¹, Shiyu Wang, James Kwok³, Yuxuan Liang¹ *

¹The Hong Kong University of Science and Technology (Guangzhou)

²University of Electronic Science and Technology of China ³The Hong Kong University of Science and Technology

{ziyuzhou30,fyclmiss,rwlinno,kwuking}@gmail.com,jamesk@cse.ust.hk,yuxliang@outlook.com

Abstract

Telemetry streams from large-scale Internet-connected systems (e.g., IoT deployments and online platforms) naturally form an irregular multivariate time series (IMTS) whose accurate forecasting is operationally vital. A closer examination reveals a defining Sparsity–Event Duality (SED) property of IMTS, i.e., long stretches with sparse or no observations are punctuated by short, dense bursts where most semantic events (observations) occur. However, existing Graph- and Transformer-based forecasters ignore SED: pre-alignment to uniform grids with heavy padding violates sparsity by inflating sequences and forcing computation at non-informative steps, while relational recasting weakens event semantics by disrupting local temporal continuity. These limitations motivate a more faithful and natural modeling paradigm for IMTS that aligns with its SED property. We find that Spiking Neural Networks meet this requirement, as they communicate via sparse binary spikes and update in an event-driven manner, aligning naturally with the SED nature of IMTS. Therefore, we present **SEDformer**, an SED-enhanced Spiking Transformer for telemetry IMTS forecasting that couples: (1) a **SED-based Spike Encoder** converts raw observations into event synchronous spikes using an **Event-Aligned LIF** neuron, (2) an **Event-Preserving Temporal Downsampling** module compresses long gaps while retaining salient firings and (3) a stack of **SED-based Spike Transformer** blocks enable intra-series dependency modeling with a membrane-based linear attention driven by EA-LIF spiking features. Experiments on public telemetry IMTS datasets show that SEDformer attains state-of-the-art forecasting accuracy while reducing energy and memory usage, providing a natural and efficient path for modeling IMTS.

Keywords

IoT Data, Irregular Telemetry Time Series Forecasting, Spiking Transformers, Spiking Neural Networks

1 Introduction

Time series are ubiquitous in large-scale Internet-connected systems, including IoT deployments and online platforms: sensor readings, device logs, service metrics, and user-facing workload signals all evolve over time and are routinely forecast to allocate resources, protect service-level agreements, and personalize user experiences [22, 27, 28, 41, 43, 56, 70]. However, in operational settings such telemetry is often irregularly sampled because activity dynamics generate bursts and lulls and measurement systems introduce uneven logging delays [1, 2, 10]. Together these factors yield observations that arrive at non-uniform intervals and are

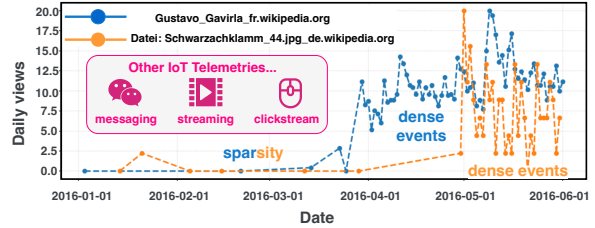


Figure 1: Five-month daily Wikipedia page views for two articles, exhibiting both sparsity and dense events. For brevity, we abbreviate the titles as “Gustavo” and “Datei”. Beyond article page views, telemetry IMTS also arises in IoT sensing, messaging, video streaming, and clickstream, where sparsity–event duality similarly holds.

asynchronous across variates, resulting in an irregular multivariate time series (IMTS) [5, 11]. Accurate telemetry IMTS forecasting is thus pivotal for capacity planning [3], anomaly response [47, 60], traffic shaping [26], and recommendation updates [9] in large-scale Internet-connected systems.

A telemetry IMTS typically consists of long stretches with few or no observations (i.e., sparse sampling), interleaved with short, dense bursts during which most semantically meaningful observations (events) occur. Fig. 1 illustrates this pattern with two Wikipedia page-view series [40]. “Gustavo” is extremely sparse from January to April, then exhibits many closely-spaced observations starting in April, while “Datei” remains sparse and spikes in May. We call this property **Sparsity–Event Duality (SED)**. Preserving event semantics while simultaneously exploiting sparsity for efficiency is a natural and effective way to model IMTS.

Deep learning models for IMTS forecasting are typically based on either Ordinary Differential Equations [6, 11, 48], Graph Neural Networks [35, 66, 67], or Transformers [7, 65]. While effective, they do not make use of the Sparsity–Event Duality. First, the IMTS is simply aligned to a regular series-level or patch-level grid, with the unobserved values replaced by zeroes [4, 5, 36, 51, 65, 66]. This results in unnecessary computations and an overly-complex model. Moreover, as all time steps (including the padded zeroes) are treated equally, this can undermine the event semantics [36, 65, 66]. Other approaches transform the IMTS to a relational structure such as point set [34] or bipartite graph [35, 61]. However, this also disrupts the continuity of local events in the time series, and the fundamental event-driven nature of IMTS is diluted or even destroyed.

Motivated by these observations, we raise the question: *Is there a naturally appropriate architecture for IMTS forecasting?* We posit that Spiking Neural Networks (SNNs) [39] might be a strong

*Yuxuan Liang is the corresponding author.

candidate. First, SNNs communicate via sparse, discrete spike trains, which are activated only when informative stimuli occur [63, 71]. This leads to substantial savings in computation and energy, and aligns with the sparse nature of IMTS where information is limited and temporally localized. Second, SNNs follow an event-driven computation paradigm [58, 62]: neurons update and emit spikes only upon events rather than at every tick of a fixed grid. This matches the event-driven nature of IMTS, where salient semantics concentrate within short, dense bursts of observations.

In this paper, we propose the **Sparsity-Event Duality** enhanced **Spiking Transformer (SEDformer)** for telemetry IMTS forecasting. We operationalize the SED of IMTS with a four-stage, end-to-end design. First, to exploit the strength of spiking neurons on sparse, event-driven IMTS, we first align the time steps between IMTS and the SNN through **SED-based Spike Encoder (SED-SE)** where the model updates only when an observation (event) arrives. At its core is an Event-Aligned LIF (EA-LIF) neuron whose leak depends on the inter-event interval, making the representation explicitly interval-aware so that long gaps decay and informative bursts dominate. Because telemetry streams contain many long idle stretches that offer little value, the **Event-Preserving Temporal Downsampling (EPTD)** module then pools along the event axis to retain whether bursts occurred while compressing extended gaps, reducing compute without reintroducing a uniform grid. On the condensed event-synchronous sequence, **SED-based Spike Transformer (SED-ST)** applies interval-conditioned, membrane-based linear attention whose scores depend on inter-event gaps, emphasizing bursts and down-weighting long silences while keeping complexity linear in the number of pooled events. Finally, a light-weight MLP-based **Query-Aware Decoder** enables query-specific forecasts. The entire architecture is trained end-to-end with mean-squared error (MSE). To the best of our knowledge, SEDformer is the first SNN-based framework for IMTS forecasting, rethinking IMTS forecasting from its defining SED property, preserving sparsity and event semantics while capturing intra-series temporal dependencies and maintaining high computational efficiency.

Our contributions can be summarized as follows:

- We identify the Sparsity-Event Duality (SED) of telemetry IMTS, arguing that preserving event semantics while exploiting sparsity is crucial for effective forecasting.
- We introduce SEDformer, which (i) aligns computation to observed events and injects interval information via the newly proposed EA-LIF neuron, (ii) compresses long gaps while preserving salient firings through max pooling, and (iii) learns intra-series temporal dependencies with a membrane-driven, irregularity-conditioned self-attention mechanism for event-aware and efficient representation learning.
- Extensive experiments on public telemetry IMTS datasets show that SEDformer outperforms the state-of-the-art in terms of both efficiency and accuracy.

2 Related Works

2.1 Telemetry & IMTS Forecasting

Telemetry forecasting spans IoT sensing, device/service metrics, and workload signals such as page views and query volumes. Classical and industry tools such as Prophet emphasize decomposable

Table 1: Comparison between prior IMTS forecasters and our proposed SEDformer.

IMTS Forecaster	Sparsity -Preserving	Event -Aligning	Energy/Cost Saving
ContiFormer [7]	✓	✓	✗
GraFITi [61]	✓	✗	✗
tPatchGNN [66]	✗	✗	✓
TimeCHEAT [35]	✗	✗	✗
HyperIMTS [32]	✓	✗	✓
KAFNet [69]	✗	✗	✓
APN [36]	✗	✗	✓
SEDformer	✓	✓	✓

trend and seasonality for large deployments [53], while early large-scale demand signals were modeled from search and query logs [8]. Popularity and traffic bursts of online content have been anticipated using early-signal dynamics and log-derived features [45, 52]. Deep learning has since become dominant: DeepAR delivers probabilistic forecasts with autoregressive RNNs at scale [49], N-BEATS advances univariate accuracy with a pure MLP stack [44], and Temporal Fusion Transformers fuse attention with multi-horizon interpretability [33]. Yet, these lines largely overlook irregular telemetry and do not explicitly model non-uniform sampling. From a broader IMTS perspective, continuous-time models parameterize temporal evolution via Differential Equation (DE): Neural ODE [6], Latent ODE [48], CRU [50], and GRU-ODE [11] with Neural Flows avoiding costly solvers [4], and ContiFormer integrating ODE dynamics with attention to report gains on irregular data [7]. Complementary relational formulations recast IMTS as graphs or sets: GraFITi uses sparse bipartite graphs [61], tPatchGNN learns transformable patches with inter-patch GNNs [66], Hi-Patch aggregates multi-scale dense variates [37], and HyperIMTS reasons over hypergraph structures [32]. However, as summarized in Tab. 1, representative methods still face limitations: DE and Transformer hybrids can be computation heavy when numerical solvers are involved, while padding-based pre-alignment to uniform grids introduces substantial zeros that inflate sequence length (violating sparsity) and blur the local event semantics central to IMTS.

2.2 SNNs for Temporal Dynamics Modeling

Early applications of Spiking Neural Networks (SNNs) to time series, as exemplified by the NeuCube framework for spatio-temporal prediction [29], relied on hand-crafted encoders or reservoir-style dynamics. With the advent of surrogate-gradient training [59], trainable spiking architectures are developed for sequential modeling. Examples include Spike-TCN [38], Spike-RNN [38], iSpikformer [38] and SpikF [58], which demonstrate the feasibility of combining SNNs with attention and Fourier representations. In parallel, researchers have sought to enhance the expressivity of spiking neurons. Several works revise the vanilla Leaky Integrate-and-Fire (LIF) neuron by incorporating richer temporal dynamics, such as STC-LIF [54] and TS-LIF [15], which aim to better capture short-term correlations and long-range dependencies. Along this line, the Learnable Multi-hierarchical (LM-H) neuron introduces learnable parameters to adaptively balance the historical and current

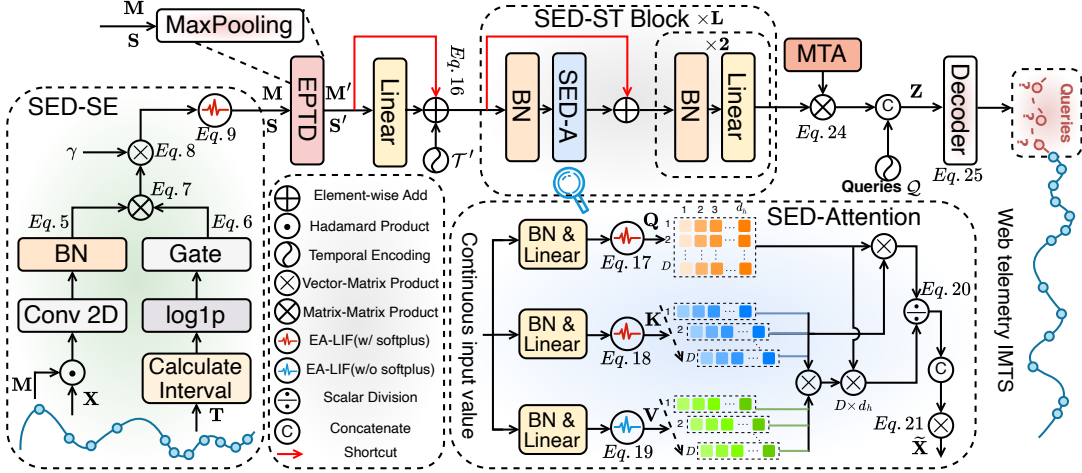


Figure 2: The architecture of SEDformer. SED-based Spike Encoder (SED-SE) initially converts IMTS into event-synchronous spike trains via an Event-Aligned LIF (EA-LIF) neuron. Event-Preserving Temporal Downsampling (EPTD) module then retains salient spikes while collapsing long gaps. A stack of SED-based Spike Transformer (SED-ST) blocks subsequently learns temporal dependencies via membrane-based SED-Attention mechanism, and Masked Time Aggregation (MTA) summarizes each variate over observed events. A lightweight Decoder finally maps the summaries to forecasts at future times.

information [19], and the multi-compartment neuron model leverages temporal dendritic heterogeneity to process multi-scale inputs [68]. Despite recent advances, most SNN-based forecasting models still assume regular sampling, leaving their application to IMTS largely underexplored. They process fixed-step sequences and do not encode inter-event intervals in neuron or attention dynamics. As a result, they overlook the irregularity typical in IMTS and compromise its Sparsity–Event Duality (SED).

3 Preliminary

3.1 Definition and Problem Formulation

Definition (IMTS and Events). We denote an irregular multivariate time series (IMTS) with D variates as $O = \{[(t_i^d, x_i^d)]_{i=1}^{L_d}\}_{d=1}^D$, where each variate d has L_d events. Each event $(t_i^d, x_i^d) \in \mathbb{R}^2$ is measured at time t_i^d and has value x_i^d . The sampling intervals in a variate are generally non-uniform (intra-variate irregularity), and event times across variates are not synchronized (inter-variate asynchrony). To obtain a global timeline, we take the union $\bigcup_{d=1}^D \{t_1^d, \dots, t_{L_d}^d\}$ and sort them as $\mathcal{T} = \{t_1 \leq \dots \leq t_K\}$. The observations are aligned along this axis to form matrices $\mathbf{T}, \mathbf{X}, \mathbf{M} \in \mathbb{R}^{K \times D}$, where $\mathbf{T}[k] = t_k$, $\mathbf{X}[k, d]$ stores the value of variate d at event t_k if observed and $\mathbf{M}[k, d] \in \{0, 1\}$ indicates that the measurement is observed at time t_k ($\mathbf{M}[k, d] = 1$) or not ($\mathbf{M}[k, d] = 0$). We refer to $(\mathbf{T}, \mathbf{X}, \mathbf{M})$ as the event-aligned representation.

Problem (IMTS Forecasting). Let $Q = \{[q_j^d]_{j=1}^{Q_d}\}_{d=1}^D$ be the matrix containing timestamps for future queries (with $q_j^d > \max_{1 \leq i \leq L_d} t_i^d$) of all the D variates. The goal is to learn a model \mathcal{F}_θ that maps historical observations O and queries Q to predictions $\hat{\mathbf{X}} = \{\hat{x}_j^d\}_{j=1}^{Q_d}\}_{d=1}^D$, where \hat{x}_j^d is the corresponding prediction at time q_j^d for variate d .

3.2 Vanilla LIF Neuron and Surrogate Gradient

The Leaky Integrate-and-Fire (LIF) [39] neuron is the canonical spiking unit in SNNs, striking a balance between biological plausibility and computational simplicity [18]. Its discrete-time dynamics comprise *integration*, *leakage*, *thresholding*, and *reset*. Specifically, at layer l , let $s^{l-1}[t] \in \{0, 1\}$ be the spike output from layer $l-1$:

$$(\text{integration}) \quad x^l[t] = W^l s^{l-1}[t], \quad (1)$$

$$(\text{leakage}) \quad m^l[t] = \alpha^l v^l[t-1] + (1 - \alpha^l) x^l[t], \quad (2)$$

$$(\text{thresholding}) \quad s^l[t] = H(m^l[t] - v_{\text{th}}), \quad (3)$$

$$(\text{reset}) \quad v^l[t] = m^l[t] - v_{\text{th}} s^l[t], \quad (4)$$

where $x^l[t]$ is the synaptic current induced by W^l , $m^l[t]$ and $v^l[t]$ are the pre- and post-spike membrane potentials, respectively, and $\alpha^l \in [0, 1]$ is the leak coefficient controlling exponential decay (setting $\alpha^l = 0$ recovers the non-leaky IF neuron). The Heaviside step function is $H(u) = 1\{u \geq 0\}$. This recurrence realizes exponentially weighted integration with leakage, acting as a low-pass memory with reset upon threshold crossing [55].

As gradients through $H(\cdot)$ are undefined, surrogate gradients are used for training [38, 42, 59]. We adopt a straight-through sigmoid estimator (STE-sigmoid) [64] and approximate $\frac{\partial H(u)}{\partial u} \approx \alpha_{\text{ste}} \sigma(\alpha_{\text{ste}} u) (1 - \sigma(\alpha_{\text{ste}} u))$, where $\sigma(\cdot)$ is the logistic sigmoid and $\alpha_{\text{ste}} > 0$ controls the slope. This enables end-to-end BPTT while leaving the forward LIF dynamics unchanged.

4 Methodology

The SEDformer framework is shown in Fig. 2. First, the SED-based Spike Encoder (SED-SE) converts IMTS into an event-aligned spike train via an Event-Aligned LIF (EA-LIF) with updates only on the observed events. The Event-Preserving Temporal Downsampling (EPTD) module then performs a temporal max-pooling on the spike

timeline. It preserves salient firing events while compressing long inter-event gaps. Next, a stack of SED-based Spike Transformer (SED-ST) blocks enable deeper representation learning of intra-series temporal irregularity. Its underlying SED-based self-attention mechanism leverages the EA-LIF-derived features conditioned on inter-event intervals. Finally, the Query-Aware Decoder addresses arbitrary forecasting queries.

4.1 SED-based Spike Encoder (SED-SE)

SNNs are naturally event-driven and sparse, making them a promising fit for IMTS. To fully exploit this property, we align the temporal axis of SNN computation with the observed events of IMTS, rather than forcing signals onto a uniform grid. Prior work for regular series aligns an SNN step with a series step by expanding each step into multiple sub-steps (e.g., Delta spike encoders [13], convolutional spike encoders [38], and ZOH upsampling [58]). These schemes assume or impose uniform sampling and thus cannot exploit irregular inter-event intervals. This motivates the proposed **SED-based Spike Encoder (SED-SE)**, which converts raw IMTS into event-synchronous sparse spike trains, preserving event semantics for downstream SNN processing.

4.1.1 SED-based Spike Encoding Process. Let $\{t_k\}_{k=1}^K$ be the non-decreasing event times (the shared index from Sec. 3.1) with inter-event intervals $\Delta t_k = t_k - t_{k-1} \geq 0$ and $\Delta t_1 = 0$, and let $\mathbf{X} \in \mathbb{R}^{K \times D}$ masked by $\mathbf{M} \in \mathbb{R}^{K \times D}$ (K is the number of events and D is the number of variates) through elementwise product \odot . Concretely, we reuse the event-aligned representation $(\mathbf{T}, \mathbf{X}, \mathbf{M})$ defined in Sec. 3.1, where $\mathbf{T}[k] = t_k$, $\mathbf{X}[k, d]$ stores the observed value of variate d at event t_k (if any), and $\mathbf{M}[k, d] \in \{0, 1\}$ indicates whether that value is observed (1) or missing (0). We feed the masked input $\mathbf{X} \odot \mathbf{M}$ to ensure that unobserved entries are not encoded. For each variate, we first extract C local channels per event to capture short-range shape around the observation while avoiding cross-variante mixing. A depthwise $1 \times k$ convolution over the masked sequence $(\mathbf{X} \odot \mathbf{M})$ aggregates a small temporal neighborhood centered at t_k , and batch normalization stabilizes the feature scale across events.*

$$\mathbf{x}^l[t_k] = \text{BN}\left(\text{Conv}_{1 \times k}((\mathbf{X} \odot \mathbf{M})[t_{k-r:k+r}])\right) \in \mathbb{R}^{D \times C}. \quad (5)$$

we subsequently inject interval information to reflect recency: longer gaps since the previous event should down-weight stale evidence, while short gaps should emphasize fresh observations. We encode this with a log-stabilized scalar gate per event:

$$\widehat{\Delta t}_k = \log\left(1 + \frac{\Delta t_k}{\rho^l}\right), \quad s_k = \sigma(a^l \widehat{\Delta t}_k + b^l), \quad (6)$$

where $\rho^l > 0$ is a learnable time scale and $a^l, b^l \in \mathbb{R}$ are learnable gate parameters. The scalar $s_k \in (0, 1)$ summarizes how recent the current event is on a normalized timeline. We then broadcast s_k over variates and channels to modulate the local features:

$$\tilde{\mathbf{x}}^l[t_k] = s_k \mathbf{x}^l[t_k], \quad \mathbf{x}^l[t_k], \tilde{\mathbf{x}}^l[t_k] \in \mathbb{R}^{D \times C}, \quad (7)$$

so that interval-aware evidence is passed downstream while preserving the event-synchronous layout. Eq. 7 injects interval awareness into the feature map while preserving its shape for downstream

* $\text{Conv}_{1 \times k}$ is depthwise across variates; k is a small odd kernel with receptive field $\{t_{k-r}, \dots, t_{k+r}\}$, $r = (k-1)/2$. $\text{BN}(\cdot)$ denotes per-channel batch normalization.

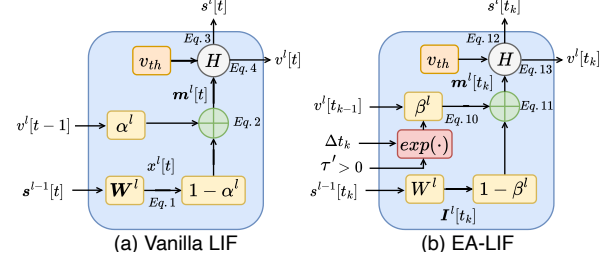


Figure 3: The structure of the (a) vanilla LIF and the (b) Event-Aligned LIF (EA-LIF) we propose.

EA-LIF processing. Then, we center and scale the gated features to obtain an event-aligned synaptic current:

$$I^l[t_k] = \gamma^l(\tilde{\mathbf{x}}^l[t_k] - \theta^l), \quad I^l[t_k] \in \mathbb{R}^{D \times C}. \quad (8)$$

Here $\gamma^l > 0$ is a learnable gain (scalar or per-channel, shared across events), and $\theta^l \in \mathbb{R}^C$ is a learnable per-channel offset that is broadcast along the variate dimension D . This operation produces a zero-referenced, amplitude-controlled current at the same event grid $\{t_k\}$. Finally, we convert these event-aligned currents into spike trains by applying the Event-Aligned LIF (EA-LIF, Sec. 4.1.2) neuron on the same event grid t_k :

$$(\mathbf{m}^l[t_k], s^l[t_k], v^l[t_k]) = \mathcal{EALIF}(v^l[t_{k-1}], I^l[t_k]; \Delta t_k, \tau^l, v_{\text{th}}) \quad (9)$$

Here, $v^l[t_{k-1}]$ denotes the previous post-spike membrane potential, $I^l[t_k]$ the event-aligned synaptic current, Δt_k the inter-event interval, τ^l the time constant, and v_{th} the firing threshold. This produces spike trains as the output of SED-SE: $\mathbf{S} = \{s^l[t_k]\}_{k=1}^K \in \mathbb{R}^{K \times D \times C}$. Practically, we use a straight-through sigmoid estimator (STE-sigmoid) to backpropagate through the binary firing in EA-LIF. In sum, SED-SE delivers an event-synchronous spike-encoding scheme that captures temporal variation and better represents the dynamic nature of IMTS.

4.1.2 Event-Aligned LIF (EA-LIF). The vanilla LIF neuron in Sec. 3.2 (Eqs. 1–4) uses a **constant** leak α^l per step, which implicitly presumes a fixed sampling interval and thus cannot reflect variable gaps between observations. To accommodate IMTS, we replace the constant leak with an interval-dependent decay that matches the continuous LIF solution: if a membrane potential follows $\frac{dv}{dt} = -\frac{1}{\tau^l}v$ between two events separated by Δt_k , then v decays multiplicatively by $\exp(-\Delta t_k/\tau^l)$. Hence we define an event-dependent leak:

$$\beta^l[t_k] = \exp\left(-\frac{\Delta t_k}{\tau^l}\right), \quad \tau^l > 0. \quad (10)$$

To ensure τ^l remains positive and trainable, we parameterize it as $\tau^l = \text{softplus}(\eta^l) + 1$, where $\text{softplus}(u) = \log(1 + e^u)$. Given the event-aligned current $I^l[t_k]$ from Eq. 8, EA-LIF updates only at event times $\{t_k\}$:

$$\mathbf{m}^l[t_k] = \beta^l[t_k] v^l[t_{k-1}] + (1 - \beta^l[t_k]) I^l[t_k], \quad (11)$$

$$s^l[t_k] = H(\mathbf{m}^l[t_k] - v_{\text{th}}), \quad (12)$$

$$v^l[t_k] = \mathbf{m}^l[t_k] - v_{\text{th}} s^l[t_k]. \quad (13)$$

Conceptually, Eqs. 12–13 have the same thresholding and reset forms as Eqs. 3–4 in vanilla LIF. The key difference is that the

decay factor $\beta^l[t_k]$ now depends on the actual inter-event gap Δt_k , and all updates are indexed on the event grid $\{t_k\}$ rather than a uniform step index t . EA-LIF is therefore naturally aligned with IMTS: computation occurs precisely at observed events (preserving event semantics), while $\beta^l[t_k]$ adapts the leakage to the elapsed time. Therefore, the state decays strongly after long silences and retains memory within dense bursts, respecting sparsity without inserting artificial time steps. It is worth noting in the special case of regular sampling ($\Delta t_k \equiv \Delta$), $\beta^l[t_k] \equiv e^{-\Delta/\tau^l}$ becomes constant, and EA-LIF reduces to vanilla LIF by identifying $\alpha^l = \beta^l[t_k]$.

4.2 Event-Preserving Temporal Downsampling

Following SED-SE, we obtain event-synchronous spikes $S \in \mathbb{R}^{K \times D \times C}$ on the shared event grid $\{t_k\}_{k=1}^K$ (Sec. 4.1). To control computation and memory while retaining event salience (the presence of spikes that mark informative observations), we downsample along the event axis via windowed max pooling, which preserves whether any spike occurs within each window and thus compresses long gaps. Let the pooling stride be $s \in \mathbb{N}$ and define $K' = \lfloor K/s \rfloor$. For pooled index $u \in \{1, \dots, K'\}$, variate $d \in \{1, \dots, D\}$, and channel $c \in \{1, \dots, C\}$, set:

$$S'[u, d, c] = \max_{k \in \{(u-1)s+1, \dots, us\}} S[k, d, c], \quad S' \in \mathbb{R}^{K' \times D \times C}. \quad (14)$$

We align pooled tokens to time by assigning the window's last event time $t'_u = t_{us}$, producing a pooled grid $\{t'_u\}_{u=1}^{K'}$. If an observation mask $M \in \{0, 1\}^{K \times D}$ accompanies the inputs, we downsample it with the same rule $M'[u, d] = \max_{k \in \{(u-1)s+1, \dots, us\}} M[k, d]$ so that a pooled position is marked observed if any event in its window is observed. This reduces the effective event length from K to K' and yields a near-linear reduction in compute and memory for the backbone while preserving within-window spike occurrences.

To keep timestamps aligned with the pooled tokens, we assign the window's last event time to the pooled position $t'_u = t_{us}, \{t'_u\}_{u=1}^{K'}$. If an observation mask $M \in \{0, 1\}^{K \times D}$ (1 if observed, 0 otherwise) accompanies the inputs, we downsample it by window-wise max so that a pooled token is marked observed if any event in its window is observed:

$$M'[u, d] = \max_{k \in \{(u-1)s+1, \dots, us\}} M[k, d], \quad M' \in \{0, 1\}^{K' \times D}. \quad (15)$$

This procedure reduces the effective event length from K to $K' = \lfloor K/s \rfloor$, yielding a near-linear reduction in compute and memory for the backbone while preserving within-window event salience. The pooled spikes S' and aligned timestamps $\{t'_u\}$ form the input sequence for the subsequent SNN backbone in Sec. 4.3, which operates directly on this event-preserving, downsampled representation.

4.3 SED-based Spike Transformer Backbone

After event-preserving downsampling (Sec. 4.2), we obtain spikes $S' \in \mathbb{R}^{K' \times D \times C}$ to represent the IMTS on the pooled event grid $\mathcal{T}' = \{t'_u\}_{u=1}^{K'}$. Subsequently, we design the temporal spiking neural network, namely SED-based Spike Transformer (SED-ST), as the backbone to model the obtained spike trains. Technically, SED-ST learns intra-series temporal representations in an event-synchronous manner: at each pooled event step u we treat the D variates as D tokens, embed their spike channels, enrich them with time, and pass the resulting $D \times d$ token matrix through L identical blocks. This design

preserves event semantics by updating only at \mathcal{T}' , and exploits sparsity with a linear-time attention whose scores are explicitly conditioned on inter-event gaps. For clarity, we omit the batch dimension B in what follows. Let $E \in \mathbb{R}^{C \times d}$ be a learnable linear projection that maps the C spike channels to the model width d (shared across variates and time), and let TE be a learnable time embedding. The token for variate d at pooled event step u is:

$$x_d[u] = E S'[u, d, :] + \text{TE}(t'_u) \in \mathbb{R}^d, \quad E \in \mathbb{R}^{C \times d}, \quad (16)$$

stacking across variates yields $X[u] = [x_1[u], \dots, x_D[u]]^\top \in \mathbb{R}^{D \times d}$, where $X[u]$ are continuous values rather than discrete spike trains.

4.3.1 SED-Attention: membrane-based linear attention. To achieve efficient computation while remaining event-aware, we combine per-head projections with EA-LIF feature maps and propose the SED-Attention (SED-A) mechanism. With H heads and $d_h = d/H$, we apply normalized projections:

$q[u] = \text{BN}_q(W_q X[u]), \quad k[u] = \text{BN}_k(W_k X[u]), \quad v[u] = \text{BN}_v(W_v X[u]),$ and split row-wise into heads $q_h[u], k_h[u], v_h[u] \in \mathbb{R}^{D \times d_h}$. We then obtain non-negative, event-aware query and key via the EA-LIF mapping (Sec. 4.1.2) on the pooled grid, with $\Delta t'_u = t'_u - t'_{u-1} \geq 0$:

$$\phi_h^{(q)}[u] = \mathcal{E}\mathcal{A}\text{-LI}\mathcal{F}^{(\text{w/ softplus})}(q_h[u]; \Delta t'_u), \quad (17)$$

$$\phi_h^{(k)}[u] = \mathcal{E}\mathcal{A}\text{-LI}\mathcal{F}^{(\text{w/ softplus})}(k_h[u]; \Delta t'_u). \quad (18)$$

For the value stream we keep the same interval-conditioned leak but omit the final non-negativity squash:

$$v_h[u] = \mathcal{E}\mathcal{A}\text{-LI}\mathcal{F}^{(\text{w/o softplus})}(v_h[u]; \Delta t'_u) \in \mathbb{R}^{D \times d_h}. \quad (19)$$

Using the standard linear-attention kernel trick [23, 30], the head-wise output at step u is:

$$y_h[u] = \frac{\phi_h^{(q)}[u] \left(\sum_{w=1}^{K'} \phi_h^{(k)}[w]^\top \tilde{v}_h[w] \right)}{(\phi_h^{(q)}[u] \sum_{w=1}^{K'} \phi_h^{(k)}[w]^\top)} \in \mathbb{R}^{D \times d_h}, \quad (20)$$

where the pre-aggregates $\sum_w \phi_h^{(k)}[w]$ and $\sum_w \phi_h^{(k)}[w]^\top \tilde{v}_h[w]$ are computed once per block. Concatenating heads and projecting:

$$Y[u] = W_o \cdot \text{Concat}_h(y_h[u]) \in \mathbb{R}^{D \times d}. \quad (21)$$

Overall complexity is linear in K' : $O(K' H d_h^2)$ where attention scores depend explicitly on $\Delta t'_u$. We drop the softmax used in vanilla self-attention, realizing both SED and linear complexity within the attention mechanism.

4.3.2 Block ordering and masked time aggregation. Each SED-ST block adopts a pre-norm Membrane Shortcut [14, 24] with two sequential updates. First, features computed by SED-A on a batch-normalized input are added back via a shortcut:

$$\tilde{X}^{(\ell)}[u] = X^{(\ell)}[u] + \text{SED-A}(\text{BN}(X^{(\ell)}[u]); \mathcal{T}'), \quad \ell = 0, \dots, L-1. \quad (22)$$

Second, a position-wise feed-forward network (FFN) is applied and added back via a shortcut to form the block output:

$$X^{(\ell+1)}[u] = \tilde{X}^{(\ell)}[u] + \text{FFN}(\text{BN}(\tilde{X}^{(\ell)}[u])). \quad (23)$$

After stacking L blocks, we perform Masked Time Aggregation (MTA) to summarize each variate over the pooled event axis while

Table 2: Forecasting results (MSE \downarrow , MAE \downarrow) of baselines and SEDformer on the sparsified Wiki2000 and WikiArticle datasets under different Sparsifying Rates. All methods use 90 historical days to predict the next 30 days. Scores are reported as mean \pm std over repeated runs with 5 different seeds. The best result in each column is shown in bold, and the second best is underlined. All numbers come from our unified re-implementation using each method's recommended settings for fair comparison.

Model	Wiki2000						WikiArticle					
	Sparsifying Rate = 25%		Sparsifying Rate = 50%		Sparsifying Rate = 75%		Sparsifying Rate = 25%		Sparsifying Rate = 50%		Sparsifying Rate = 75%	
Metric	MSE $\times 10^{-3}$	MAE $\times 10^{-2}$	MSE $\times 10^{-2}$	MAE $\times 10^{-2}$	MSE $\times 10^{-2}$	MAE $\times 10^{-2}$	MSE $\times 10^{-3}$	MAE $\times 10^{-2}$	MSE $\times 10^{-2}$	MAE $\times 10^{-2}$	MSE $\times 10^{-2}$	MAE $\times 10^{-2}$
Neural ODE	13.50 \pm 0.02	8.06 \pm 0.12	2.27 \pm 0.06	11.10 \pm 0.12	3.33 \pm 0.07	13.50 \pm 0.02	9.52 \pm 0.12	6.43 \pm 0.01	2.13 \pm 0.07	9.26 \pm 0.08	3.63 \pm 0.06	11.33 \pm 0.04
Latent ODE	13.40 \pm 0.04	7.76 \pm 0.06	1.58 \pm 0.04	9.52 \pm 0.02	2.40 \pm 0.06	12.02 \pm 0.12	9.93 \pm 0.06	7.46 \pm 0.10	1.39 \pm 0.05	7.46 \pm 0.04	2.09 \pm 0.02	9.41 \pm 0.05
GRU-ODE	10.28 \pm 0.03	7.21 \pm 0.11	1.69 \pm 0.04	9.35 \pm 0.13	2.35 \pm 0.08	11.62 \pm 0.03	9.38 \pm 0.11	6.58 \pm 0.02	2.08 \pm 0.06	9.41 \pm 0.09	2.65 \pm 0.07	11.28 \pm 0.05
GRU-D	10.55 \pm 0.02	8.12 \pm 0.15	2.41 \pm 0.08	9.95 \pm 0.10	3.48 \pm 0.09	9.91 \pm 0.04	9.67 \pm 0.13	6.48 \pm 0.03	2.05 \pm 0.05	9.73 \pm 0.11	2.48 \pm 0.05	9.65 \pm 0.06
SeFT	10.23 \pm 0.03	6.52 \pm 0.10	2.08 \pm 0.04	11.88 \pm 0.14	3.12 \pm 0.06	12.76 \pm 0.05	8.95 \pm 0.09	7.01 \pm 0.04	2.35 \pm 0.09	8.84 \pm 0.07	1.91 \pm 0.08	8.98 \pm 0.03
RainDrop	13.72 \pm 0.05	8.38 \pm 0.13	1.89 \pm 0.03	10.73 \pm 0.09	3.47 \pm 0.10	14.15 \pm 0.06	9.21 \pm 0.14	6.96 \pm 0.02	2.28 \pm 0.08	9.58 \pm 0.10	3.29 \pm 0.04	11.87 \pm 0.07
Warpformer	13.04 \pm 0.02	8.67 \pm 0.09	2.12 \pm 0.07	9.45 \pm 0.11	2.98 \pm 0.05	10.28 \pm 0.03	9.16 \pm 0.10	6.75 \pm 0.03	1.97 \pm 0.04	9.02 \pm 0.06	2.81 \pm 0.09	9.99 \pm 0.02
mTAND	9.98 \pm 0.03	9.22 \pm 0.09	1.95 \pm 0.06	8.31 \pm 0.03	2.89 \pm 0.11	9.45 \pm 0.12	10.34 \pm 0.05	8.12 \pm 0.11	2.03 \pm 0.03	7.45 \pm 0.05	2.18 \pm 0.04	9.01 \pm 0.05
CRU	11.25 \pm 0.02	9.40 \pm 0.08	1.80 \pm 0.05	8.03 \pm 0.02	2.68 \pm 0.10	9.10 \pm 0.11	10.02 \pm 0.04	7.78 \pm 0.10	1.86 \pm 0.02	7.12 \pm 0.04	2.01 \pm 0.03	8.68 \pm 0.04
Neural Flow	10.35 \pm 0.03	8.32 \pm 0.09	1.76 \pm 0.06	7.12 \pm 0.12	2.20 \pm 0.08	8.90 \pm 0.16	10.12 \pm 0.05	7.12 \pm 0.08	1.66 \pm 0.02	6.90 \pm 0.05	1.91 \pm 0.04	8.18 \pm 0.06
tPatchGNN	9.88 \pm 0.03	5.89 \pm 0.11	1.49 \pm 0.12	6.68 \pm 0.12	<u>1.85 \pm 0.10</u>	<u>8.60 \pm 0.12</u>	8.81 \pm 0.10	5.38 \pm 0.08	<u>1.18 \pm 0.03</u>	<u>6.10 \pm 0.06</u>	1.83 \pm 0.05	7.89 \pm 0.05
GraFTi	9.65 \pm 0.08	6.20 \pm 0.06	1.60 \pm 0.02	7.02 \pm 0.10	1.90 \pm 0.06	8.81 \pm 0.06	9.62 \pm 0.04	6.02 \pm 0.06	1.46 \pm 0.04	6.61 \pm 0.03	1.90 \pm 0.03	8.12 \pm 0.08
TimeCHEAT	10.35 \pm 0.12	6.01 \pm 0.08	1.72 \pm 0.04	7.08 \pm 0.03	2.02 \pm 0.04	9.80 \pm 0.10	10.02 \pm 0.08	6.12 \pm 0.04	1.60 \pm 0.06	7.12 \pm 0.06	2.20 \pm 0.03	8.03 \pm 0.06
KAFNet	9.79 \pm 0.19	5.75 \pm 0.12	<u>1.44 \pm 0.03</u>	6.78 \pm 0.23	1.86 \pm 0.04	8.66 \pm 0.23	9.10 \pm 0.16	5.37 \pm 0.08	1.19 \pm 0.02	6.23 \pm 0.06	1.88 \pm 0.02	7.92 \pm 0.07
HyperIMTS	<u>9.42 \pm 0.03</u>	<u>5.40 \pm 0.10</u>	1.56 \pm 0.22	<u>6.64 \pm 0.07</u>	1.90 \pm 0.04	8.70 \pm 0.03	<u>8.80 \pm 0.06</u>	<u>5.30 \pm 0.08</u>	1.25 \pm 0.09	6.15 \pm 0.08	<u>1.78 \pm 0.01</u>	<u>7.88 \pm 0.08</u>
SEDformer	9.19 \pm 0.13	5.24 \pm 0.11	1.36 \pm 0.22	6.44 \pm 0.17	1.81 \pm 0.02	8.53 \pm 0.02	8.71 \pm 0.26	5.21 \pm 0.09	1.15 \pm 0.18	6.00 \pm 0.18	1.69 \pm 0.02	7.84 \pm 0.05

Table 3: Statistical significance test results (paired t-test) comparing SEDformer against the second-best method HyperIMTS. P-values less than 0.05 indicate statistically significant improvements.

Dataset	Wiki2000						WikiArticle					
	Sparsifying Rate = 25%		Sparsifying Rate = 50%		Sparsifying Rate = 75%		Sparsifying Rate = 25%		Sparsifying Rate = 50%		Sparsifying Rate = 75%	
Metric	MSE	MAE										
P-value	0.038	0.021	0.015	0.032	0.008	0.003	0.042	0.028	0.012	0.019	0.002	0.045

avoiding bias from unobserved steps. Using $\mathbf{M}' \in \{0, 1\}^{K' \times D}$:

$$\mathbf{z}[d] = \frac{\sum_{u=1}^{K'} \mathbf{M}'[u, d] \mathbf{X}^{(L)}[u, d, :]}{\sum_{u=1}^{K'} \mathbf{M}'[u, d]} \in \mathbb{R}^d, \quad d = 1, \dots, D. \quad (24)$$

This aggregation uses only observed events (entries with $\mathbf{M}'[u, d] = 1$), respecting irregular sampling and preventing missing windows from diluting the representation. Therefore, MTA produces a length-agnostic, missingness-robust summary aligned to the event grid, providing a compact input for downstream prediction.

4.4 Query-Conditioned Decoder

4.4.1 Answering the Queries. After event irregularity has been compressed by the EPTD module and intra-series dependencies have been refined by the L stacked SED-ST blocks, our model outputs the representation $\mathbf{Z} \in \mathbb{R}^{D \times d}$; its j -th row \mathbf{z}_j is a compact summary of variate j . For each query time $q_j^{(r)}$, we concatenate this summary with its learnable time embedding and map the result to a scalar prediction via an MLP:

$$\hat{x}_r^j = \text{MLP}(\mathbf{z}_j \oplus \text{TE}(q_j^{(r)})), \quad j = 1, \dots, D, \quad r = 1, \dots, Q_j. \quad (25)$$

The head is query-conditioned (each output depends on its own query time) and parallelizable across all (j, r) , while remaining lightweight since all cross-time interactions are handled upstream.

4.4.2 Training objective. Given ground-truth values $\{x_r^j\}$ at the query times $\{q_j^{(r)}\}$, we minimize mean squared error (MSE) averaged over variates and their queries:

$$\mathcal{L} = \frac{1}{D} \sum_{j=1}^D \frac{1}{Q_j} \sum_{r=1}^{Q_j} \left(\hat{x}_r^j - x_r^j \right)^2. \quad (26)$$

5 Experiments

5.1 Experimental Setup

5.1.1 Datasets. We experiment on two widely used public telemetry IMTS benchmarks (originating from web-traffic telemetry) that exhibit long missing spans and bursty event patterns common in Internet-connected telemetry streams. **Wiki2000** [17]: daily page-view counts for 9,013 Wikipedia pages. We use the TFB release [46] and select the first 200 variates. **WikiArticle** [40]: the Kaggle *Web Traffic Time Series Forecasting* set; we load `train_1.csv` and keep the first 300 variates. We restrict to 200/300 series to ensure parity of training cost across baselines and reproducibility; choosing the “first” in the provider’s order avoids cherry-picking and yields a fixed, bias-free subset. Both raw corpora contain long missing spans and sporadic anomalies that make direct forecasting ill-posed. Following common benchmarking practice, we first create a clean reference trajectory per variate on a regular daily grid and then introduce irregularity in a controlled way [57]. Concretely, we perform local gap filling via second-order Lagrange interpolation and

mild outlier smoothing, and subsequently “sparsify” the cleaned series by independently masking observations at rates 25%/50%/75%. This simulation of data sparsity via independent, random masking corresponds to the Missing Completely at Random (MCAR) mechanism, a standard and foundational approach in benchmarking literature for creating controlled, unbiased evaluation scenarios [25]. This two-step protocol has been used to evaluate IMTS models under controlled irregular sampling while keeping the latent signal fixed for fair comparison [12, 57]. It also aligns with continuous-time evaluations that simulate non-uniform sampling or random deletions [16, 48]. We refer to the masking rate as the “Sparsifying Rate”, and introduce the detailed procedure of constructing these datasets in Appendix A. We adopt a multi-step setting: a 90-day history window is used to forecast the next 30 days.

5.1.2 Baselines. Telemetry streams are naturally sparse and irregularly sampled, with large missing observations and non-uniform intervals. **Unlike prior works that treat them as dense continuous streams [7], the IMTS formulation explicitly models discrete events with irregular timestamps and better captures their true structure.** Following the standard IMTS forecasting setting (Sec. 2.1), we treat telemetry forecasting as an **offline sequence-to-sequence** problem (Sec. 3.1) and evaluate SEDformer against strong IMTS baselines from four methodological classes. (i) RNN-based: GRU-D [5]. (ii) Differential Equation-based: Neural ODE [6], Latent ODE [48], GRU-ODE [11], CRU [50], and Neural Flow [4]. (iii) Transformer- and Attention-based: ContiFormer [7], Warpformer [65], mTAND [51], SeFT [20], and KAFNet [69]. (iv) GNN- and Set-based: RainDrop [67], GraFITi [61], tPatchGNN [66], TimeCHEAT [35], and HyperIMTS [32]. For methods originally proposed for IMTS interpolation (e.g., mTAND [51]), we swap interpolation targets for queries to enable extrapolation. For methods originally proposed for IMTS classification (e.g., SeFT [20], Warpformer [65]), we replace the classification head with a MLP forecasting head so that all baselines output real-valued trajectories under the same training objective. A detailed introduction is provided in Appendix B.

5.1.3 Implementation Details. We run all experiments on a single NVIDIA RTX 3090 GPU. Training uses the Adam optimizer [31]. Model quality is reported with two standard metrics, MSE and MAE, computed over the set of queried timestamps Q as $\text{MSE} = \frac{1}{|Q|} \sum_{i=1}^{|Q|} (x_i - \hat{x}_i)^2$, $\text{MAE} = \frac{1}{|Q|} \sum_{i=1}^{|Q|} |x_i - \hat{x}_i|$. Here x_i and \hat{x}_i denote the ground truth and the prediction at the i -th query, respectively, and $|Q|$ is the number of queries. The complete hyperparameter grids and selection protocol are provided in Appendix C.

5.2 Main Results

We summarize the full comparisons in Tab. 2. Overall, SEDformer attains the strongest accuracy across both datasets under a wide range of Sparsifying Rates, with the gains most pronounced in the medium-to-high sparsity regimes that best reflect real telemetry streams. We attribute this advantage to three design aspects: (i) Sparsity Awareness: the model naturally consumes irregular observations with event-aware encoding rather than relying on heavy imputation, thus avoiding bias from ad hoc gap-filling; (ii)

Multi-scale Temporal Modeling: local bursts and long-range seasonalities are jointly captured, which is crucial when observations are asynchronous and event-driven; and (iii) Cross-series Consolidation with Robustness: shared structure is leveraged without over-smoothing individual series, improving stability across seeds. In contrast, families tailored to regular grids (e.g., pure patching [66] or warping Transformers [65]) underutilize time gaps and degrade as sparsity increases; missingness-handling RNNs [5, 50] encode gaps but struggle to maintain long-range dependencies and cross-series transfer; and graph-based baselines [61] help under moderate sparsity but may assume denser contexts and thus plateau at higher sparsity. We also conduct repeated runs and two-sided significance tests comparing SEDformer against the strongest baseline per setting; the p -values in Tab. 3 indicate statistically reliable improvements in multiple regimes and comparable performance elsewhere, confirming that SEDformer provides optimal forecasting under real telemetry IMTS while remaining stable in easier settings.

5.3 Efficiency Analysis

As illustrated in Fig. 4, we evaluate efficiency on Wiki2000 with a sparsifying rate of 25%, using the same batch size (16) across all models for fairness. We compare three representative baselines that cover dominant IMTS paradigms: tPatchGNN [66] (patch-level padding), KAFNet [69] (series-level padding), and GraFITi [61] (bipartite graph without padding). Training time is measured as wall-clock time per epoch on the same GPU stack; our SNN is trained with standard surrogate gradients, enabling straightforward timing. SEDformer uses the fewest parameters and, via event-aligned computation, requires substantially fewer operations than GNN-based methods while remaining comparable to a lightweight ANN baseline. For energy, we follow established digital cost accounting [15, 21, 38]: total energy sums memory and arithmetic costs weighted by operation counts, using FLOPs for ANNs and SOPs for SNNs under a 45 nm technology model. Under this setting, SEDformer reduces theoretical energy by over $80\times$ vs. tPatchGNN [66], $47\times$ vs. GraFITi [61], and $15\times$ vs. KAFNet [69]. These results suggest that event-synchronous spiking can preserve accuracy while markedly improving energy efficiency. Details of the energy accounting are provided in Appendix D, and additional results across datasets and sparsifying rates are in Appendix E.

5.4 Spike Trains Visualization

To concretize how spike encoders behave on irregular data, Fig. 5 shows spike trains from three representatives on the same synthetic IMTS: a Delta Spike encoder (vanilla LIF) [38], a Convolutional Spike encoder (vanilla LIF) [38], and our SED-based Spike Encoder (SED-SE with EA-LIF). The two grid-based encoders implicitly assume uniform sampling, so their spikes are quantized to the fixed grid: in the long sparse stretch they miss isolated observations, and around the burst they either emit a few delayed, clustered spikes (Delta) or smear short bursts into wide plateaus with shifted on/off transitions (Convolutional), thus blurring and desynchronizing event timing while offering no gain other than longer, costlier sequences under zero-padding. In contrast, SED-SE updates only on the irregular event grid and modulates leak by the inter-event interval. Long gaps induce strong decay and silence, whereas dense

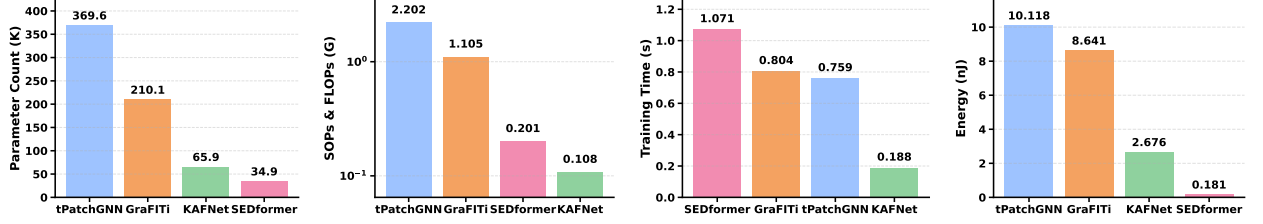


Figure 4: Efficiency analysis on the Wiki2000 dataset with Sparsifying Rate = 25%. “OPs” refers to SOPs in SNN and FLOPs in ANN. “SOPs” is the synaptic operations of SEDformer. “FLOPs” denotes the floating point operations of other ANN baselines.

Table 4: Ablation results of SEDformer on two datasets evaluated by MSE and MAE (mean±std). The best results are in bold.

Dataset	Wiki2000						WikiArticle					
	Sparsifying Rate = 25%		Sparsifying Rate = 50%		Sparsifying Rate = 75%		Sparsifying Rate = 25%		Sparsifying Rate = 50%		Sparsifying Rate = 75%	
	MSE $\times 10^{-3}$	MAE $\times 10^{-2}$	MSE $\times 10^{-2}$	MAE $\times 10^{-2}$	MSE $\times 10^{-2}$	MAE $\times 10^{-2}$	MSE $\times 10^{-3}$	MAE $\times 10^{-2}$	MSE $\times 10^{-2}$	MAE $\times 10^{-2}$	MSE $\times 10^{-2}$	MAE $\times 10^{-2}$
SEDformer	9.19 ± 0.13	5.24 ± 0.11	1.36 ± 0.22	6.44 ± 0.17	1.81 ± 0.02	8.53 ± 0.02	8.71 ± 0.26	5.21 ± 0.09	1.15 ± 0.18	6.00 ± 0.18	1.69 ± 0.02	7.84 ± 0.05
w/o SED-SE	10.91 ± 0.03	5.51 ± 0.07	2.60 ± 0.03	6.91 ± 0.06	1.96 ± 0.10	8.92 ± 0.08	10.08 ± 0.04	6.56 ± 0.08	1.47 ± 0.03	6.20 ± 0.05	2.26 ± 0.05	8.52 ± 0.05
w/o EA-LIF & w/ LIF	10.95 ± 0.03	6.03 ± 0.05	1.70 ± 0.04	7.78 ± 0.02	2.55 ± 0.10	8.85 ± 0.09	9.78 ± 0.05	7.62 ± 0.10	1.78 ± 0.03	6.89 ± 0.05	1.92 ± 0.04	8.52 ± 0.02
w/o EPTD	10.98 ± 0.02	6.09 ± 0.04	1.74 ± 0.05	7.88 ± 0.03	2.61 ± 0.11	8.96 ± 0.12	9.81 ± 0.04	7.63 ± 0.11	1.80 ± 0.02	6.99 ± 0.04	1.95 ± 0.03	8.55 ± 0.05
w/o SED-ST	11.08 ± 0.02	6.18 ± 0.04	1.76 ± 0.05	7.94 ± 0.03	2.63 ± 0.11	9.01 ± 0.12	10.29 ± 0.03	7.68 ± 0.11	1.82 ± 0.02	7.03 ± 0.04	2.27 ± 0.04	8.76 ± 0.05
w/o SED-A & w/ SA	10.81 ± 0.03	6.25 ± 0.08	1.69 ± 0.04	7.75 ± 0.02	2.54 ± 0.10	8.83 ± 0.11	9.65 ± 0.05	7.49 ± 0.10	1.75 ± 0.03	6.86 ± 0.05	1.96 ± 0.05	8.42 ± 0.04

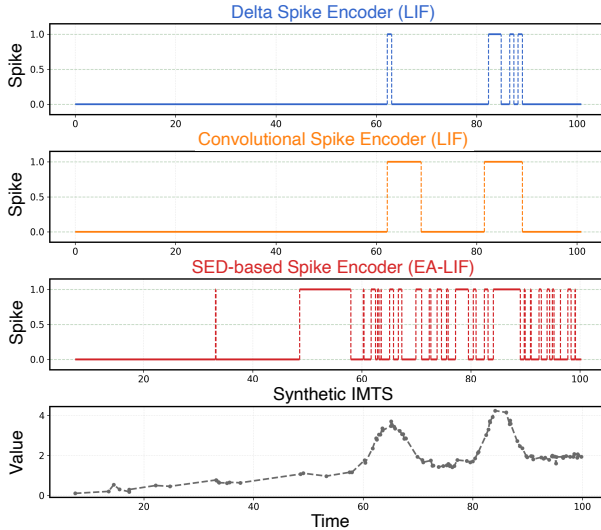


Figure 5: Spike trains generated by Delta Spike Encoder and Convolutional Spike Encoder with vanilla LIF neuron, as well as the proposed SED-based Spike Encoder with EA-LIF.

bursts produce concentrated spikes exactly at observation times. This event-synchronous, interval-aware behavior preserves event semantics, exploits sparsity without grid padding, and aligns with the Sparsity–Event Duality that underpins IMTS, explaining the empirical advantages of our model. We describe the procedure for constructing the synthetic IMTS dataset in Appendix F.

5.5 Ablation Study

We conduct ablations across all datasets and Sparsifying Rates to assess the contribution of each component. As summarized in Tab. 4, removing any module consistently degrades accuracy, confirming that each stage is functionally necessary. The largest drop arises when the SED-ST blocks are removed, highlighting the importance of modeling temporal irregularity and performing deep representation learning directly on the event-synchronous sequence. Substituting the EA-LIF with the vanilla LIF also hurts performance, indicating that conditioning leakage on inter-event intervals is crucial for irregular data. Likewise, replacing SED-A with standard Self-Attention (SA) leads to consistent declines, showing that our membrane-driven, interval-aware attention better preserves event semantics while exploiting sparsity. These results validate the design choices that align computation with observed events and encode inter-event timing throughout the stack.

5.6 Hyper-parameter Analysis

We study the sensitivity of SEDformer to four key hyper-parameters, results are summarized in Fig. 6. A moderate leak yields the best accuracy across datasets, whereas too small τ over-reacts to noise in dense bursts and too large τ retains stale context across long gaps, confirming the need to balance event persistence and inter-event decay. Smaller strides preserve more event detail and generally improve performance; overly aggressive pooling compresses long gaps but also removes short bursts, degrading accuracy. Increasing the number of backbone blocks helps at first (better temporal representation) and then saturates, with a shallow sweet spot that avoids overfitting and keeps compute modest. Enlarging the width improves capacity up to a point, after which returns diminish and variance grows, suggesting that a mid-range dimension offers a

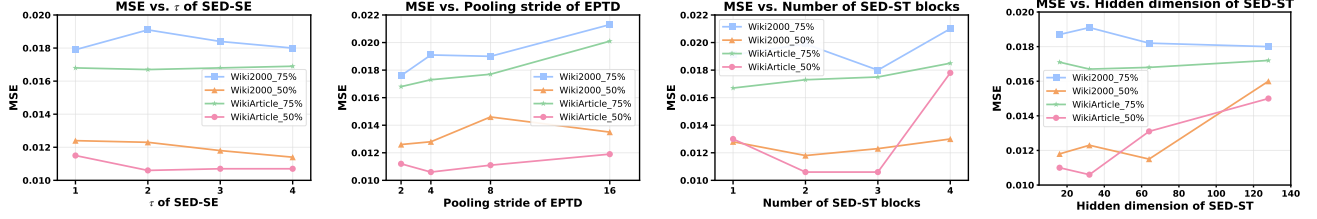


Figure 6: Hyper-parameter sensitivity analysis of SEDformer evaluated by MSE on time constant τ of SED-SE, pooling stride of EPTD module, number of SED-ST blocks, hidden dimension of SED-ST.

good trade-off between expressiveness and efficiency. Overall, SEDformer is robust in a broad region around these mid-range settings, and the observed trends align with our design intuition: respect events (avoid over-pooling), forget across long gaps (appropriate τ), and favor compact yet sufficiently deep backbones.

6 Conclusion and Future Work

We present SEDformer, a Spiking Transformer that models irregular telemetry time series by aligning computation to observed events and conditioning dynamics on inter-event intervals (which is identified and summarized as the Sparsity–Event Duality, SED). The proposed SEDformer integrates an SED-based Spike Encoder, Event–Preserving Temporal Downsampling module, and a stack of SED-based Spike Transformer blocks, which together preserve event semantics while exploiting sparsity for efficiency. Experiments on public telemetry datasets demonstrate that this event-synchronous, interval-conditioned approach delivers state-of-the-art accuracy with reduced compute and energy, while our analyses show that grid-padding pipelines and relational recastings tend to dilute short bursts by inflating sequences and disrupting local temporal continuity. Limitations of SEDformer are discussed in Appendix G. Looking ahead, we plan to extend the model with probabilistic forecasting and calibration for risk-aware operations, study online learning for streaming settings with distribution shift, and explore deployment on low-power hardware and neuromorphic backends to obtain practical efficiency gains.

References

- [1] Tyler Akidau, Alex Balikov, Kaya Bekiroglu, Slava Chernyak, Josh Haberman, Reuven Lax, Sam McVeety, Daniel Mills, Paul Nordstrom, and Sam Whittle. 2013. MillWheel: Fault-Tolerant Stream Processing at Internet Scale. In *Proceedings of the VLDB Endowment*.
- [2] Tyler Akidau, Robert Bradshaw, Craig Chambers, Slava Chernyak, Rafael J Fernández-Moctezuma, Reuven Lax, Sam McVeety, Daniel Mills, Frances Perry, Eric Schmidt, et al. 2015. The Dataflow Model: A Practical Approach to Balancing Correctness, Latency, and Cost in Massive-Scale, Unbounded, Out-of-Order Data Processing. In *Proceedings of the VLDB Endowment*.
- [3] Virgilio A. F. Almeida and Daniel A. Menasce. 2002. Capacity Planning: An Essential Tool for Managing Web Services. *IT Professional* (2002).
- [4] Marin Bilos, Johanna Sommer, Syama Sundar Rangapuram, Tim Januschowski, and Stephan Günnemann. 2021. Neural Flows: Efficient Alternative to Neural ODEs. In *Advances in Neural Information Processing Systems*.
- [5] Zhengping Che, Sanjay Purushotham, Kyunghyun Cho, David Sontag, and Yan Liu. 2018. Recurrent Neural Networks for Multivariate Time Series with Missing Values. *Scientific Reports* (2018).
- [6] Tian Qi Chen, Yulia Rubanova, Jesse Bettencourt, and David Duvenaud. 2018. Neural Ordinary Differential Equations. In *Advances in Neural Information Processing Systems*.
- [7] Yuqi Chen, Kan Ren, Yansen Wang, Yuchen Fang, Weiwei Sun, and Dongsheng Li. 2023. ContiFormer: Continuous-Time Transformer for Irregular Time Series Modeling. In *Advances in Neural Information Processing Systems*.
- [8] Hyunyoung Choi and Hal Varian. 2012. Predicting the Present with Google Trends. *Economic Record* (2012).
- [9] Paul Covington, Jay Adams, and Emre Sargin. 2016. Deep Neural Networks for YouTube Recommendations. In *ACM Conference on Recommender Systems*.
- [10] Mark E Crovella and Azer Bestavros. 2002. Self-Similarity in World Wide Web Traffic: Evidence and Possible Causes. *IEEE/ACM Transactions on Networking* (2002).
- [11] Edward De Brouwer, Jaak Simm, Adam Arany, and Yves Moreau. 2019. GRU-ODE-Bayes: Continuous Modeling of Sporadically-Observed Time Series. In *Advances in Neural Information Processing Systems*.
- [12] Wenjie Du, Jun Wang, Linglong Qian, Yiyuan Yang, Fanxing Liu, Zepu Wang, Zina Ibrahim, Haoxin Liu, Zhiyuan Zhao, Yingjie Zhou, Wenjia Wang, Kaize Ding, Yuxuan Liang, B. Aditya Prakash, and Qingsong Wen. 2024. TSI-Bench: Benchmarking Time Series Imputation. *arXiv preprint arXiv:2406.12747* (2024).
- [13] Jason K. Eshaghian, Max Ward, Emre O. Neftci, Xinxin Wang, Gregor Lenz, Girish Dwivedi, Mohammed Bennamoun, Doo Seok Jeong, and Wei D. Lu. 2023. Training Spiking Neural Networks Using Lessons from Deep Learning. *Proc. IEEE* (2023).
- [14] Yuetong Fang, Deming Zhou, Ziqing Wang, Hongwei Ren, ZeCui Zeng, Lusong Li, Shibo Zhou, and Renjing Xu. 2025. Spiking Transformers Need High Frequency Information. In *Advances in Neural Information Processing Systems*.
- [15] Shibo Feng, Wanjin Feng, Xingyu Gao, Peilin Zhao, and Zhiqi Shen. 2025. TS-LIF: A Temporal Segment Spiking Neuron Network for Time Series Forecasting. In *International Conference on Learning Representations*.
- [16] Vincent Fortuin, Dmitry Baranchuk, Gunnar Raetsch, and Stephan Mandt. 2020. GP-VAE: Deep Probabilistic Time Series Imputation. In *International Conference on Artificial Intelligence and Statistics*.
- [17] Jan Gasthaus, Konstantinos Benidis, Yuyang Wang, Syama Sundar Rangapuram, David Salinas, Valentin Flunkert, and Tim Januschowski. 2019. Probabilistic Forecasting with Spline Quantile Function RNNs. In *International Conference on Artificial Intelligence and Statistics*.
- [18] Wolfram Gerstner, Werner M. Kistler, Richard Naud, and Liam Paninski. 2014. *Neuronal Dynamics: From Single Neurons to Networks and Models of Cognition*. Cambridge University Press.
- [19] Zecheng Hao, Xinyu Shi, Zihan Huang, Tong Bu, Zhaofei Yu, and Tiejun Huang. 2023. A Progressive Training Framework for Spiking Neural Networks with Learnable Multi-Hierarchical Model. In *International Conference on Learning Representations*.
- [20] Max Horn, Michael Moor, Christian Bock, Bastian Rieck, and Karsten M. Borgwardt. 2020. Set Functions for Time Series. In *International Conference on Machine Learning*.
- [21] Mark Horowitz. 2014. Computing's Energy Problem (And What We Can Do About It). In *IEEE International Solid-State Circuits Conference*.
- [22] Min Hou, Chang Xu, Zhi Li, Yang Liu, Weiqing Liu, Enhong Chen, and Jiang Bian. 2022. Multi-Granularity Residual Learning with Confidence Estimation for Time Series Prediction. In *ACM Web Conference*.
- [23] Jiaxi Hu, Yongqi Pan, Jusen Du, Disen Lan, Xiaqiang Tang, Qingsong Wen, Yuxuan Liang, and Weigao Sun. 2025. Comba: Improving Bilinear RNNs with Closed-Loop Control. *arXiv preprint arXiv:2506.02475*.
- [24] Yifan Hu, Lei Deng, Yujie Wu, Man Yao, and Guoqi Li. 2025. Advancing Spiking Neural Networks Toward Deep Residual Learning. *IEEE Transactions on Neural Networks and Learning Systems* (2025).
- [25] Sebastian Jäger, Arndt Allhorn, and Felix Bießmann. 2021. A Benchmark for Data Imputation Methods. *Frontiers in Big Data* (2021).
- [26] Sushant Jain, Alok Kumar, Subhasree Mandal, Joon Ong, Leon Poutievski, Arjun Singh, Subbaiah Venkata, Jim Wanderer, Junlan Zhou, Min Zhu, et al. 2013. B4: Experience with a Globally-Deployed Software Defined WAN. *ACM SIGCOMM Computer Communication Review* (2013).
- [27] Sheo Yon Jhin, Jaehoon Lee, Minju Jo, Seungji Kook, Jinsung Jeon, Jihyeon Hyeong, Jayoung Kim, and Noseong Park. 2022. EXIT: Extrapolation and Interpolation-Based Neural Controlled Differential Equations for Time-Series Classification and Forecasting. In *ACM Web Conference*.
- [28] Renhe Jiang, Zhaonan Wang, Yudong Tao, Chuang Yang, Xuan Song, Ryosuke Shibusaki, Shu-Ching Chen, and Mei-Ling Shyu. 2023. Learning Social Meta-Knowledge for Nowcasting Human Mobility in Disaster. In *ACM Web Conference*.
- [29] Nikola K. Kasabov. 2014. NeuCube: A Spiking Neural Network Architecture for Mapping, Learning and Understanding of Spatio-Temporal Brain Data. *Neural Networks* (2014).
- [30] Angelos Katharopoulos, Apoorv Vyas, Nikolaos Pappas, and François Fleuret. 2020. Transformers are rnns: Fast autoregressive transformers with linear attention. In *International Conference on Machine Learning*.
- [31] Diederik P. Kingma and Jimmy Ba. 2014. Adam: A Method for Stochastic Optimization. *arXiv preprint arXiv:1412.6980*.
- [32] Boyuan Li, Yicheng Luo, Zhen Liu, Junhao Zheng, Jianming Lv, and Qianli Ma. 2025. HyperIMTS: Hypergraph Neural Network for Irregular Multivariate Time Series Forecasting. In *International Conference on Machine Learning*.
- [33] Bryan Lim, Sercan Ö Arik, Nicolas Loeff, and Tomas Pfister. 2021. Temporal Fusion Transformers for Interpretable Multi-Horizon Time Series Forecasting. *International Journal of Forecasting* (2021).
- [34] Shengsheng Lin, Weiwei Lin, Wentai Wu, Haojun Chen, and Junjie Yang. 2024. SparseTSF: Modeling Long-Term Time Series Forecasting with 1k Parameters. In *International Conference on Machine Learning*.
- [35] Jiexi Liu, Meng Cao, and Songcan Chen. 2025. TimeCHEAT: A Channel Harmony Strategy for Irregularly Sampled Multivariate Time Series Analysis. In *AAAI Conference on Artificial Intelligence*.
- [36] Xuyuan Liu, Xiangfei Qiu, Xingjian Wu, Zhengyu Li, Chenjuan Guo, Jilin Hu, and Bin Yang. 2025. Rethinking Irregular Time Series Forecasting: A Simple yet Effective Baseline. *arXiv preprint arXiv:2505.11250*.
- [37] Yicheng Luo, Bowen Zhang, Zhen Liu, and Qianli Ma. 2025. Hi-Patch: Hierarchical Patch GNN for Irregular Multivariate Time Series. In *International Conference on Machine Learning*.
- [38] Changze Lv, Yansen Wang, Dongqi Han, Xiaoqing Zheng, Xuanjing Huang, and Dongsheng Li. 2024. Efficient and Effective Time-Series Forecasting with Spiking Neural Networks. In *International Conference on Machine Learning*.
- [39] Wolfgang Maass. 1997. Networks of Spiking Neurons: The Third Generation of Neural Network Models. *Neural Networks* (1997).
- [40] Maggie, Oren Anava, Vitaly Kuznetsov, and Will Cukierski. 2017. Web Traffic Time Series Forecasting. Kaggle.
- [41] Kentaro Miyake, Hiroyoshi Ito, Christos Faloutsos, Hirotomo Matsumoto, and Atsuyuki Morishima. 2024. NetEvolve: Social Network Forecasting Using Multi-Agent Reinforcement Learning with Interpretable Features. In *ACM Web Conference*.
- [42] Emre O. Neftci, Hesham Mostafa, and Friedemann Zenke. 2019. Surrogate Gradient Learning in Spiking Neural Networks: Bringing the Power of Gradient-Based Optimization to Spiking Neural Networks. *IEEE Signal Processing Magazine* (2019).
- [43] Wentao Ning, Reynold Cheng, Xiao Yan, Ben Kao, Nan Huo, Nur Al Hasan Haldar, and Bo Tang. 2024. Debiasing Recommendation with Personal Popularity. In *ACM Web Conference*.
- [44] Boris N. Oreshkin, Dmitrii Carpow, Nicolas Chapados, and Yoshua Bengio. 2019. N-BEATS: Neural Basis Expansion Analysis for Interpretable Time Series Forecasting. *arXiv preprint arXiv:1905.10437* (2019).
- [45] Henrique Pinto, Jussara M. Almeida, and Marcos A. Gonçalves. 2013. Using Early View Patterns to Predict the Popularity of YouTube Videos. In *ACM International Conference on Web Search and Data Mining*.
- [46] Xiangfei Qiu, Jilin Hu, Lekui Zhou, Xingjian Wu, Junyang Du, Buang Zhang, Chenjuan Guo, Aoying Zhou, Christian S. Jensen, Zhenli Sheng, and Bin Yang. 2024. TFB: Towards Comprehensive and Fair Benchmarking of Time Series Forecasting Methods. *Proceedings of the VLDB Endowment* (2024).
- [47] Hansheng Ren, Bixiong Xu, Yujing Wang, Chao Yi, Congrui Huang, Xiaoyu Kou, Tony Xing, Mao Yang, Jie Tong, and Qi Zhang. 2019. Time-Series Anomaly Detection Service at Microsoft. In *ACM SIGKDD Conference on Knowledge Discovery and Data Mining*.
- [48] Yulia Rubanova, Tian Qi Chen, and David Duvenaud. 2019. Latent Ordinary Differential Equations for Irregularly-Sampled Time Series. In *Advances in Neural Information Processing Systems*.
- [49] David Salinas, Valentin Flunkert, Jan Gasthaus, and Tim Januschowski. 2020. DeepAR: Probabilistic Forecasting with Autoregressive Recurrent Networks. *International Journal of Forecasting* (2020).

- [50] Mona Schirmer, Mazin Eltayeb, Stefan Lessmann, and Maja Rudolph. 2022. Modeling Irregular Time Series with Continuous Recurrent Units. In *International Conference on Machine Learning*.
- [51] Satya Narayan Shukla and Benjamin M. Marlin. 2021. Multi-Time Attention Networks for Irregularly Sampled Time Series. In *International Conference on Learning Representations*.
- [52] Gabor Szabo and Bernardo A. Huberman. 2010. Predicting the Popularity of Online Content. *Commun. ACM* (2010).
- [53] Sean J. Taylor and Benjamin Letham. 2018. Forecasting at Scale. *The American Statistician* (2018).
- [54] Lihao Wang and Zhaofei Yu. 2024. Autaptic Synaptic Circuit Enhances Spatio-Temporal Predictive Learning of Spiking Neural Networks. *arXiv preprint arXiv:2406.00405* (2024).
- [55] Lihao Wang and Zhaofei Yu. 2024. Autaptic Synaptic Circuit Enhances Spatio-Temporal Predictive Learning of Spiking Neural Networks. *arXiv preprint arXiv:2406.00405*.
- [56] Yanyun Wang, Dehuo Du, Haibo Hu, Zi Liang, and Yuanhao Liu. 2024. TS Fool: Crafting Highly-Imperceptible Adversarial Time Series Through Multi-Objective Attack. *arXiv preprint arXiv:2209.06388*.
- [57] Yannick Wölker, Christian Beth, Matthias Renz, and Arne Biastoch. 2023. SUSTeR: Sparse Unstructured Spatio Temporal Reconstruction on Traffic Prediction. In *ACM International Conference on Advances in Geographic Information Systems*.
- [58] Wenjie Wu, Dexuan Huo, and Hong Chen. 2025. SpikF: Spiking Fourier Network for Efficient Long-Term Prediction. In *International Conference on Machine Learning*.
- [59] Yujie Wu, Lei Deng, Guoqi Li, Jun Zhu, Yuan Xie, and Luping Shi. 2019. Direct Training for Spiking Neural Networks: Faster, Larger, Better. In *AAAI Conference on Artificial Intelligence*.
- [60] Yongzheng Xie, Hongyu Zhang, and Muhammad Ali Babar. 2025. Multivariate Time Series Anomaly Detection by Capturing Coarse-Grained Intra- and Inter-Variate Dependencies. In *ACM Web Conference*.
- [61] Vijaya Krishna Yalavarthi, Kiran Madhusudhanan, Randolph Scholz, Nourhan Ahmed, Johannes Burchert, Shayan Jawed, Stefan Born, and Lars Schmidt-Thieme. 2024. GraFITi: Graphs for Forecasting Irregularly Sampled Time Series. In *AAAI Conference on Artificial Intelligence*.
- [62] Man Yao, Jiakui Hu, Zhaokun Zhou, Li Yuan, Yonghong Tian, Bo Xu, and Guoqi Li. 2023. Spike-Driven Transformer. *arXiv preprint arXiv:2307.01694*.
- [63] Man Yao, Guangshe Zhao, Hengyu Zhang, Yifan Hu, Lei Deng, Yonghong Tian, Bo Xu, and Guoqi Li. 2023. Attention Spiking Neural Networks. *IEEE Transactions on Pattern Analysis and Machine Intelligence* (2023).
- [64] Friedemann Zenke and Surya Ganguli. 2018. SuperSpike: Supervised Learning in Multilayer Spiking Neural Networks. *Neural Computation* (2018).
- [65] Jiawen Zhang, Shun Zheng, Wei Cao, Jiang Bian, and Jia Li. 2023. Warpformer: A Multi-Scale Modeling Approach for Irregular Clinical Time Series. In *ACM SIGKDD Conference on Knowledge Discovery and Data Mining*.
- [66] Weijia Zhang, Chenlong Yin, Hao Liu, Xiaofang Zhou, and Hui Xiong. 2024. Irregular Multivariate Time Series Forecasting: A Transformable Patching Graph Neural Networks Approach. In *International Conference on Machine Learning*.
- [67] Xiang Zhang, Marko Zeman, Theodoros Tsiligkaridis, and Marinka Zitnik. 2022. Graph-Guided Network for Irregularly Sampled Multivariate Time Series. In *International Conference on Learning Representations*.
- [68] Hanle Zheng, Zhong Zheng, Rui Hu, Bo Xiao, Yujie Wu, Fangwen Yu, Xue Liu, Guoqi Li, and Lei Deng. 2024. Temporal Dendritic Heterogeneity Incorporated with Spiking Neural Networks for Learning Multi-Timescale Dynamics. *Nature Communications* (2024).
- [69] Ziyu Zhou, Yiming Huang, Yanyun Wang, Yuankai Wu, James Kwok, and Yuxuan Liang. 2026. Revitalizing Canonical Pre-Alignment for Irregular Multivariate Time Series Forecasting. In *AAAI Conference on Artificial Intelligence*.
- [70] Ziyu Zhou, Gengyu Lyu, Yiming Huang, Zihao Wang, Ziyu Jia, and Zhen Yang. 2024. SDformer: Transformer with Spectral Filter and Dynamic Attention for Multivariate Time Series Long-Term Forecasting. In *International Joint Conference on Artificial Intelligence*.
- [71] Zhaokun Zhou, Yuesheng Zhu, Chao He, Yaowei Wang, Shuicheng YAN, Yonghong Tian, and Li Yuan. 2023. Spikformer: When Spiking Neural Network Meets Transformer. In *International Conference on Learning Representations*.

Appendix

A Additional Details on Dataset Construction

Corpora. We use two public telemetry IMTS benchmarks that originate from web-traffic telemetry: Wiki2000 [17] and WikiArticle [40]. For Wiki2000 we follow TFB [46] and keep the first 200 variates (daily, 2015-07-01–2017-09-10). For WikiArticle we load `train_1.csv` and keep the first 300 variates (daily, 2015-07-01–2016-12-31). Choosing the provider’s first 200/300 series ensures parity of training cost and avoids cherry-picking bias.

Protocol. Raw series contain long gaps and sporadic outliers. We first create a clean reference trajectory per variate on the daily grid, then induce irregular sampling via independent masking (MCAR) [25], following common IMTS benchmarking practice [12, 16, 48, 57]. We evaluate in a rolling multi-step setting with a 90-day history and 30-day horizon; sparsifying rates $r \in \{0.25, 0.50, 0.75\}$ use a fixed seed across methods. The complete cleaning–sparsifying pipeline is summarized in Alg. 1.

Algorithm 1 Telemetry benchmarks: Clean \rightarrow MCAR sparsify (per variate)

Input: $x \in \mathbb{R}^T$ (daily); window w ; gap cap L_{\max} ; outlier τ ; rate r ; seed s
Output: \tilde{x} on irregular times **or** (\tilde{x}, m) with $m \in \{0, 1\}^T$

- 1: $\tilde{x} \leftarrow x$
- 2: *Short gaps* ($\leq L_{\max}$): quadratic Lagrange; else boundary bridge
- 3: *Outliers*: with median μ , MAD σ , if $|\tilde{x}_t - \mu|/\sigma > \tau$ then replace by local median (size w)
- 4: Spline-impute any remaining long gaps
- 5: RNG $\leftarrow s$; sample $m_t \sim \text{Bernoulli}(1 - r)$ i.i.d.
- 6: **return** $\tilde{x} = \{(t, \tilde{x}_t) : m_t = 1\}$ **or** (\tilde{x}, m)

B Baselines

- **Neural ODE** [6]: Views hidden dynamics as a continuous-time ODE and integrates forward with an ODE solver; forecasts are obtained by decoding states at queried times.
- **Latent ODE** [48]: Encodes an irregular history into an initial latent state, evolves it with a neural ODE, and decodes values at arbitrary future timestamps, enabling fully continuous-time forecasting.
- **GRU-ODE** [11]: Maintains a GRU state that decays according to elapsed time between events and is updated only at observation times, combining event-driven updates with continuous-time evolution.
- **GRU-D** [5]: A GRU with learnable time decay and feature-wise imputation; uses masks and time gaps to modulate hidden updates under missingness and irregular intervals.
- **SeFT** [20]: Treats samples as an unordered set of (time, value, variable tuples and aggregates with permutation-invariant set functions (Deep Sets) for irregular inputs.
- **RainDrop** [67]: Builds a time-aware graph over observations and applies message passing with temporal attention to fuse information across irregular stamps and variables.
- **Warpformer** [65]: Learns a timestamp/value warping to align multi-scale patterns before Transformer encoding, improving robustness to nonuniform sampling.

- **mTAND** [51]: Learns continuous-time embeddings via attention over reference points; for forecasting, replaces interpolation queries by future queries to obtain predictions at desired times.
- **CRU** [50]: Uses continuous recurrent units derived from linear SDE dynamics with continuous–discrete filtering, providing principled uncertainty handling for irregular streams.
- **Neural Flows** [4]: Reparameterizes neural-ODE trajectories as continuous normalizing flows to improve stability/efficiency while retaining continuous-time flexibility.
- **tPatchGNN** [66]: Forms transformable temporal patches per series, models intra-patch patterns with a Transformer, and uses time-adaptive GNNs to capture inter-variable relations.
- **GraFITi** [61]: Constructs a time- and variable-aware graph directly on unaligned observations; stacked diffusion/attention operators propagate signals to infer future values without pre-alignment.
- **TimeCHEAT** [35]: Enforces channel harmony by combining channel-dependent graph convolutions within patches with channel-independent Transformers across patches, balancing specialization and sharing.
- **KAFNet** [69]: Revitalizes canonical pre-alignment via a lightweight kernel-alignment/feature pre-alignment module that maps irregular series to a unified temporal basis, enabling simple yet competitive forecasting on unaligned data.
- **HyperIMTS** [32]: Models IMTS as a hypergraph where observations are nodes and temporal/variable hyperedges capture higher-order dependencies; message passing occurs directly on irregular event sets.

C Hyper-parameters Search Space

We sweep the following hyperparameters for our model:

- τ in SED-SE: $\tau \in \{1, 2, 3, 4\}$.
- Pooling stride of EPTD: $s \in \{2, 4, 8, 16\}$.
- Number of SED-ST blocks: $L \in \{1, 2, 3, 4\}$.
- Hidden dimension in SED-ST: $d \in \{16, 32, 64, 128\}$.

D Theoretical Energy Consumption Calculation

We follow standard digital cost accounting [15, 38] with Horowitz’s 45 nm energy model [21]. For a model with layers \mathcal{L} , the theoretical energy is

$$E_{\text{tot}} = \sum_{\ell \in \mathcal{L}} \left(N_{\text{MAC}}^{(\ell)} e_{\text{MAC}} + N_{\text{add}}^{(\ell)} e_{\text{add}} + N_{\text{rd}}^{(\ell)} e_{\text{rd}} + N_{\text{wr}}^{(\ell)} e_{\text{wr}} \right),$$

where e_{MAC} , e_{add} are operation energies and e_{rd} , e_{wr} are SRAM read-/write energies under 45 nm where $e_{\text{MAC}} = 4.6 \text{ pJ}$ and $e_{\text{add}} = 0.9 \text{ pJ}$.

ANN layers. For a dense linear (or 1×1 conv) with $d_{\text{in}} \times d_{\text{out}}$ and effective sequence length T_{eff} , $N_{\text{MAC}} = d_{\text{in}} d_{\text{out}} T_{\text{eff}}$ and $N_{\text{add}} \approx d_{\text{out}} (d_{\text{in}} - 1) T_{\text{eff}}$; memory terms account for parameter fetches and activations. With MCAR masking, grid-based models still process the full grid so $T_{\text{eff}} = T$, whereas true event-driven models use $T_{\text{eff}} = |\{t_k : m_k = 1\}|$.
SNN (event-driven). For a spiking layer with fan-in d_{in} and spike count S_{ℓ} , a spike-operation (SOP) bundles an accumulate, a compare/reset, and a few SRAM accesses:

$$E_{\text{SNN}}^{(\ell)} = S_{\ell} (e_{\text{acc}} + e_{\text{cmp}} + e_{\text{rd}} + e_{\text{wr}}) + E_{\text{params}}^{(\ell)},$$

with $S_{\ell} \approx \rho_{\ell} |\{t_k : m_k = 1\}| d_{\text{out}}$ given firing rate ρ_{ℓ} . SEDformer is event-aligned (counts scale with observed events), so its OPs/SOPs

and energy shrink with sparsity. Under the same 45 nm assumptions, this yields the large theoretical savings reported in Fig. 4 (e.g., $> 80\times$ vs. tPatchGNN [66], $47\times$ vs. GraFITi [61], and $15\times$ vs. KAFNet [69]).

E Additional Efficiency Analysis

To substantiate the efficiency claims in Sec. 5.3, we report additional results on higher sparsifying rates in Fig. 7. We follow the same accounting protocol as the main text (45 nm digital energy model with Horowitz costs; SOPs for SNNs and FLOPs for ANNs; identical GPU, batch size = 16, and software stack). Across both datasets and masking levels, SEDformer consistently achieves markedly lower theoretical energy than representative ANN baselines. The gap generally widens as sparsity increases, reflecting that event-synchronous computation scales with the number of pooled events rather than the length of a padded grid, thereby avoiding work on non-informative steps.

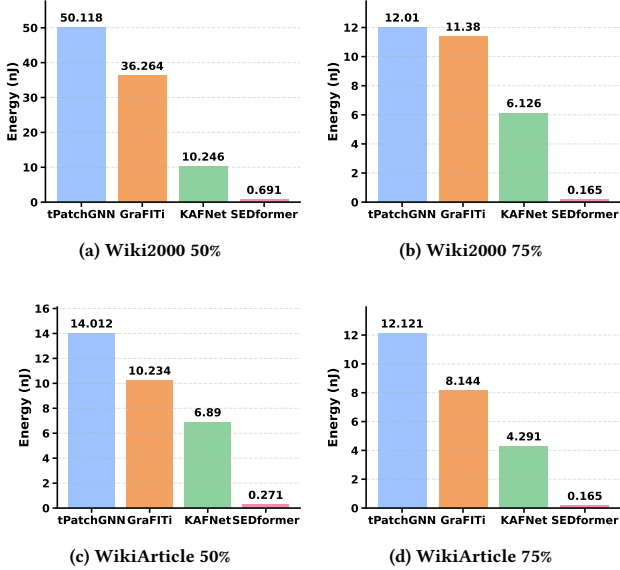


Figure 7: Extended energy comparison under higher sparsity. Theoretical energy is computed using the same digital cost model as Sec. 5.3 (Horowitz 45 nm), with SOPs for SEDformer and FLOPs for ANN baselines. SEDformer retains a consistent advantage across datasets and sparsifying rates, and the margin tends to increase as sparsity grows, highlighting the benefit of event-synchronous computation.

F Spike-Encoder Visualization Dataset

To visualize spike encoders (Sec. 5.4), we synthesize an irregular multivariate time series on a single channel. Let $f(t)$ be a smooth baseline with two bursts; we sample (i) a *sparse* phase on $[0, 60]$ with n_s points and (ii) a *dense* phase on $(60, T]$ with n_d points ($T=100$, seed fixed). Observed values are $x_k = f(t_k) + \epsilon_k$ with small Gaussian noise. We also build a regular grid $\{t_k^{\text{reg}}\}_{k=1}^N$ and its values $x_k^{\text{reg}} = f(t_k^{\text{reg}}) + \epsilon_k$ to run grid-based encoders.

Encoders. (i) *Delta (regular)*: $s_k^{\Delta} = \mathbf{1}(|x_k^{\text{reg}} - x_{k-1}^{\text{reg}}| \geq \theta)$. (ii) *Convolutional (regular)*: $y = \kappa * x^{\text{reg}}$ with a short kernel κ ; $s_k^{\text{conv}} = \mathbf{1}((y_k - \bar{y}) / \text{std}(y) \geq \tau_c)$. (iii) *SED-SE (irregular, EA-LIF)*: for irregular stamps $\{t_k\}$, $\beta_k = \exp(-\frac{t_k - t_{k-1}}{\tau})$, $m_k = \beta_k v_{k-1} + (1 - \beta_k) \gamma(x_k - \theta)$, $s_k = \mathbf{1}(m_k \geq v_{\text{th}})$, $v_k = m_k - v_{\text{th}} s_k$. We re-implement the Delta and the Convolutional spike encoders from [38]. Grid encoders quantize to the fixed step, which blurs timing under sparsity; SED-SE fires exactly at observation times and modulates leak by inter-event intervals, yielding event-synchronous behavior.

G Discussions and Limitations

Our proposed SEDformer broadens the IMTS forecasting toolkit by demonstrating that spiking neural networks can deliver energy-efficient, robust, and accurate predictions. We hope it offers a fresh perspective to the data mining and time-series community and stimulates further research on event-native modeling of irregular telemetry streams. Moreover, SEDformer’s event-synchronous computation aligns naturally with bursty, asynchronous telemetry (e.g., page views, service metrics, sensors, and device logs), preserving the information of real observation events rather than padded grid steps. Our event-synchronous spiking design with interval-aware leakage also has limitations. First, its practical efficiency hinges on kernels and runtimes that exploit irregular timestamps; on dense tensor backends the sparsity benefits may be underutilized. Second, our training and evaluation primarily assume MCAR-style sparsity; under MNAR or structured censoring the model can behave suboptimally without retraining or auxiliary propensity/imputation mechanisms. Third, spike thresholds, leak constants and interval scalings couple to dataset-specific sampling rates, so cross-dataset transfer may require careful retuning to avoid under-/over-firing. Finally, our energy accounting follows standard 45 nm digital cost models and reports theoretical, not measured, consumption; absolute numbers will vary with hardware and low-level implementations even if the relative trends remain.